Applied Catalysis B: Environmental 243 (2019) 330–336

Contents lists available at ScienceDirect

Applied Catalysis B: Environmental

journal homepage: www.elsevier.com/locate/apcatb

Phase and interlayer effect of transition metal dichalcogenide cocatalyst toward photocatalytic hydrogen evolution: The case of $MoSe_2$

Jianjian Yi[a], Hongping Li[a], Yongji Gong[b], Xiaojie She[a], Yanhua Song[c], Yuanguo Xu[a], Jiujun Deng[a], Shouqi Yuan[a], Hui Xu[a,*], Huaming Li[a]

[a] School of the Environment and Safety Engineering, Institute for Energy Research, Jiangsu University, Zhenjiang, 212013, PR China
[b] School of Materials Science and Engineering, Beihang University, Beijing, 100191, PR China
[c] School of Environmental and Chemical Engineering, Jiangsu University of Science and Technology, Zhenjiang, 212013, PR China

ARTICLE INFO

Keywords:
Photocatalysis
Hydrogen evolution
Cocatalyst
Metallic
Interlayer expansion

ABSTRACT

Visible-light-driven photocatalytic hydrogen evolution reaction (HER) is of far-reaching significance to address the energy and environmental issues. Owing to the seriously limited charge separation and surface catalytic conversion efficiency, cocatalyts especially noble-metals (e.g. Pt) are fundamentally required for this reaction. Transitional metal dichalcogenides (TMDs) represent a type of promising nonprecious cocatalysts, but they still lack effective strategies to optimize the performance. In this work, we report a rational design of $MoSe_2$ to form interlayer-expanded 1T-phase structure, to maximize the cocatalytic activity for photocatalytic HER by optimizing the surface activation ability for reaction molecule at both edge and basal sites. In a practical photocatalytic reaction, when intergrated with a semiconductor (two-dimensional carbon nitride, 2D-C_3N_4), the hybrid exhibits a satisfactory hydrogen evolution rate (1672.6 μmol g^{-1} h^{-1}, with external quantum efficiency of 5.2% at 420 nm) that greatly higher than the normal spacing 2H-$MoSe_2$ (186.7 μmol g^{-1} h^{-1}) and most noble-metals (e.g. Au, Ag, Pd). The giant improved HER performance strongly demonstrates the superiority of the presented phase and interlayer engineering strategy. The formation mechanism of the specialized structure and the key factor affecting the performance are also discussed. This work may provide new avenues for the design of TMDs-based catalysts toward HER application.

1. Introduction

Photocatalytic hydrogen evolution reaction (HER) represents a highly promising approach to address the current environmental and energy crisis. However, its realization is still a mirage for the negligible solar to energy conversion efficiency [1–3]. Among various strategies to develop high-efficiency photocatalytic systems, the integration of semiconductors with cocatalysts is widely designed [4–8]. The positive roles of cocatalyst in photocatalytic HER primarily include (i) promoting the separation of electron-hole (e–h) pairs and (ii) providing dense active sites for H_2 evolution [9,10]. Platinum (Pt) has been demonstrated to be the unbeatable cocatalyst for photocatalytic water splitting for its large work function and zero-approaching adsorption/desorption free energy of hydrogen ($\Delta G_{H^*} \approx 0$) [5,11]. However, the expensive material cost would limit its large-scale application. In general, an ideal cocatalyst for photocatalytic HER should possess the merits of efficient charge trapping and molecule activation ability, along with the low-cost and stable feature.

The observation of the catalytic activity of MoS_2 edge makes it possible to replace Pt using earth-abundant transitional metal dichalcogenides (TMDs), particularly MX_2 (M═Mo or W, X═S or Se) [11–13]. Two primary drawbacks of MX_2 are that the density of active sites is limited to edge sites and the electrical conductivity is not satisfied for effective charge migration, both of which would restrict their potential to rival to the Pt-group or other state-of-the-art catalysts for catalytic HER [14–16]. Phase engineering of MX_2 from the pristine semiconducting 2H phase (trigonal prismatic coordination) to metallic 1T phase (octahedral coordination) (Fig. S1) with dense active sites and enhanced conductivity is considered as an effective pathway to tackle these shortcomings [17]. In a typical photocatalytic reaction, the advantage of 1T-MX_2 as cocatalyts originated from two aspects: (i) the active sites of MX_2 for HER locate at both the edge and basal sites, unlike the limited active edge sites in the 2H counterpart; and (ii) the enhanced conductivity of 1T-MX_2 provides higher mobility for the migration of photogenerated electrons from the semiconductors [9,18–20]. Besides the phase engineering, recent studies reveal that the

* Corresponding author.
E-mail address: xh@ujs.edu.cn (H. Xu).

https://doi.org/10.1016/j.apcatb.2018.10.054
Received 14 July 2018; Received in revised form 13 September 2018; Accepted 22 October 2018
Available online 24 October 2018
0926-3373/

interlayer engineering of MX_2 to form interlayer expanded structure is an additional strategy for enhancing the HER performance [21]. It has shown that the interlayer-expanded MoS_2 (0.94 nm) possesses increased H* adsorption on the edge sites supported by theoretical calculations, thus enhancing the final HER performance [22]. Similarly, DFT calculation demonstrates that the ΔG_{H^*} of MoS_2 reduced from 0.149 eV to -0.052 eV, a more preferable value close to thermoneutral ($\Delta G_{H^*} \approx 0$), with the interlayer spacing increasing from 0.62 nm to 0.95 nm [23]. Such interlayer engineering can provide MX_2 faster hydrogen adsorption and desorption process, which is preferable for excellent HER performance. As the most popular MX_2 material, MoS_2 has made the most comprehensive research and advance [4,18,24–26]. Soon afterwards, the intrinsic HER activity of pristine 2H-$MoSe_2$ has been realized [27–29]. As contrast, $MoSe_2$ still lacks systematic research especially in photocatalysis, and there is still great space for improving the HER performance, requiring rational structural design such as synergistic phase and interlayer engineering to optimize the performance.

In this work, we describe a bottom-up solvothermal method using octylamine as solvent to synthesize interlayer-expanded 1T-$MoSe_2$ in-situ grown on 2D-C_3N_4 semiconductor. In our case, the introduction of octylamine molecules may play a vital role for the formation of interlayer-expanded 1T phase structure: (i) embedding into the layers of $MoSe_2$ to expand the interlayer spacing and (ii) serving as electron donor to induce phase transition from semiconducting 2H to metallic 1T phase. As cocatalyst, the interlayer-expanded 1T-$MoSe_2$ modified 2D-C_3N_4 exhibits significantly enhanced HER performance of 1672.6 μmol g^{-1} h^{-1} with apparent quantum efficiency of 5.2%, greatly higher than the normal spacing 2H-$MoSe_2$ obtained by in-situ annealing treatment of the former (186.7 μmol g^{-1} h^{-1}) and most state-of-the-art cocatalysts. Given the comparable light absorbance and charge kinetics of interlayer-expanded 1T-$MoSe_2$/2D-C_3N_4 and normal spacing 2H-$MoSe_2$/2D-C_3N_4, the performance gap between the two catalysts can be ascribed to the different phase and interlayer structure induced different surface catalytic conversion efficiency. The presented structural design strategy here is expected to be widely used to synthesize novel structured catalysts based on TMDs in the future.

2. Experimental section

2.1. Chemicals

$MoCl_5$ (> 99.6% metals basis, Aladdin) and SeO_2 (> 99.9% metals basis, Aladdin) were used in the synthesis. All other chemicals were of analytical grade and purchased from Sinopharm Chemical Reagent Co., Ltd. (China). All of the chemicals were used directly without any purication. The Argon was purchased from Jiangsu SOPO (group) co., Ltd. The water used in all the experiments was de-ionized (DI).

2.2. Preparation of the samples

Synthesis of interlay-expanded 1T-$MoSe_2$/2D-C_3N_4 (MSCN(IE/1T)) and interlayer-expanded 1T-$MoSe_2$ (MS(IE/1T)): 8.0 mg of $MoCl_5$ and 6.5 mg of SeO_2 were dissolved or dispersed in 5 mL octylamine respectively. 30 mg of 2D-C_3N_4 were dispersed in 10 mL octylamine in a 25 mL Teflon-lined autoclave and kept stirring. Afterwards, 400 μL of $MoCl_5$ solution and SeO_2 dispersion were injected into the autoclave. After stirring for several minutes, the autoclave was kept in an oven at 180 °C for 12 h, then cooled down to room temperature. The product was collected and washed using absolute ethanol and distilled water several times, and freeze-dried. The preparation of MS(IE/1T) is similar to that of the hybrid, except for the addition of 2D-C_3N_4 [30].

Synthesis of normal spacing 2H-$MoSe_2$/2D-C_3N_4 (MSCN(NS/2H)) and normal spacing 2H-$MoSe_2$ (MS(NS/2H)): The MS(NS/2H) and MSCN(NS/2H) were obtained by annealing as-prepared MS(IE/1T) and MSCN(IE/1T) samples at 400 °C in Ar atmosphere for 1 h with a heating rate of 10 °C/min.

2.3. Photocatalytic activity measurement

The photocatalytic hydrogen evolution reaction was carried out in an online system (LbSolar-3AG, PerfectLight, Beijing). 10 mg of photocatalyst powder was dispersed in 100 mL of aqueous solution containing 10 mL of triethanolamine as hole sacrificial and 90 mL water. The solution was then thoroughly degassed and irradiated by a 300 W Xenon lamp (PLS-SXE 300C (BF), Perfectlight, Beijing) with an optical filter ($\lambda > 400$ nm). The reaction temperature was controlled at 10 °C by cooling water circular system to avoid photothermal effect. The photocatalytic H_2 formation was measured using an online gas chromatograph (GC D7900 P, TCD detector Ar carrier, 5 Å molecular sieve column). The apparent quantum efficiency was measured by applying a Xe lamp (300 W) with 420, 435 and 450 nm band pass filters (PerfectLight, Beijing). The number of incident photons was measured using a radiant power energy meter (I400, PerfectLight, Beijing).

The detail about synthetic method of pure 2D-C_3N_4 and other 2D-C_3N_4-based reference materials, characterization techniques, calculation for external quantum efficiency and theoretical calculations are shown in Supplementary information.

3. Results and discussion

The preparation route of different $MoSe_2$ cocatalyst based photocatalytic systems is illustrated in Fig. 1a. Firstly, the g-C_3N_4 with typical 2D structure (denoted as 2D-C_3N_4, as shown in Fig. 1c and S2) was chosen as the model semiconductor to exam the cocatalytic activity of $MoSe_2$. The large specific area and flexibility are beneficial for the uniform loading of cocatalyst, while the sheet like structure shortens the distance of charge migration, both of which contribute to understand the behavior of cocatalysts well. In the process to prepare interlayer-expanded 1T-$MoSe_2$/2D-C_3N_4 (MSCN(IE/1T)), firstly, the precursor can form Mo-octylamine and Se-octylamine coordination complexes and adsorb onto the surface of 2D-C_3N_4. Then the surface loaded $MoSe_2$ can be obtained after solvothermal reaction. During the process, the octylamine can first adsorb on the surface of atom-layer, and then, along with crystal growth to multilayer structure, octylamine will embed into the interlayer of $MoSe_2$ to expand the interlayer distance [31]. The octylamine could also serve as the electron donor to induce phase transition to 1T phase. More detailed mechanism for the formation of the special structure will be proven in the following. Meanwhile, in comparison with previous physical assembly of two separate materials [18,20,25,32,33], the presented in-situ growth route can construct a more intimate interface for charge migration. To demonstrate the superiority of the interlayer-expanded 1T structure, the normal interlayer spacing 2H-$MoSe_2$/2D-C_3N_4 (MSCN(NS/2 H)) was prepared by annealing on MSCN(IE/1T) to extract the embedded molecules and induce phase transition to the stable 2H phase.

The X-ray diffraction (XRD) patterns of the samples all display similar characteristic diffraction peak located at 27.7° corresponding to the (002) facet of pure 2D-C_3N_4, indicating the structure of 2D-C_3N_4 is well preserved after loading $MoSe_2$ (Fig. 1b). The signal of $MoSe_2$ is not detected owing to the low loading amount and crystallinity (Fig. S3). The morphology of the catalysts was observed by transmission electron microscopy (TEM). From the images of MSCN(IE/1T) and MSCN(NS/2H) (Fig. 1d, e), the $MoSe_2$ cocatalysts in similar nanoisland structure uniformly distribute over the surface of 2D-C_3N_4. It is worth noting that the hybrids obtained through in-situ growth exhibit uniform dispersion of $MoSe_2$, in comparison with the bare $MoSe_2$ (Fig. S4), which is largely aggregated to form cluster. This observation indicates that 2D-C_3N_4 is a good platform for the growth and dispersion of $MoSe_2$.

With the increase of magnification, it can be observed that the $MoSe_2$ on 2D-C_3N_4 possesses typical layered structure of TMDs, comprised of 5–8 layers with an interlayer distance of 1.17 nm (Fig. 2a) which is higher than the normal spacing $MoSe_2$ samples (~0.65 nm) [28,29]. This result directly confirms that the interlayer-expanded

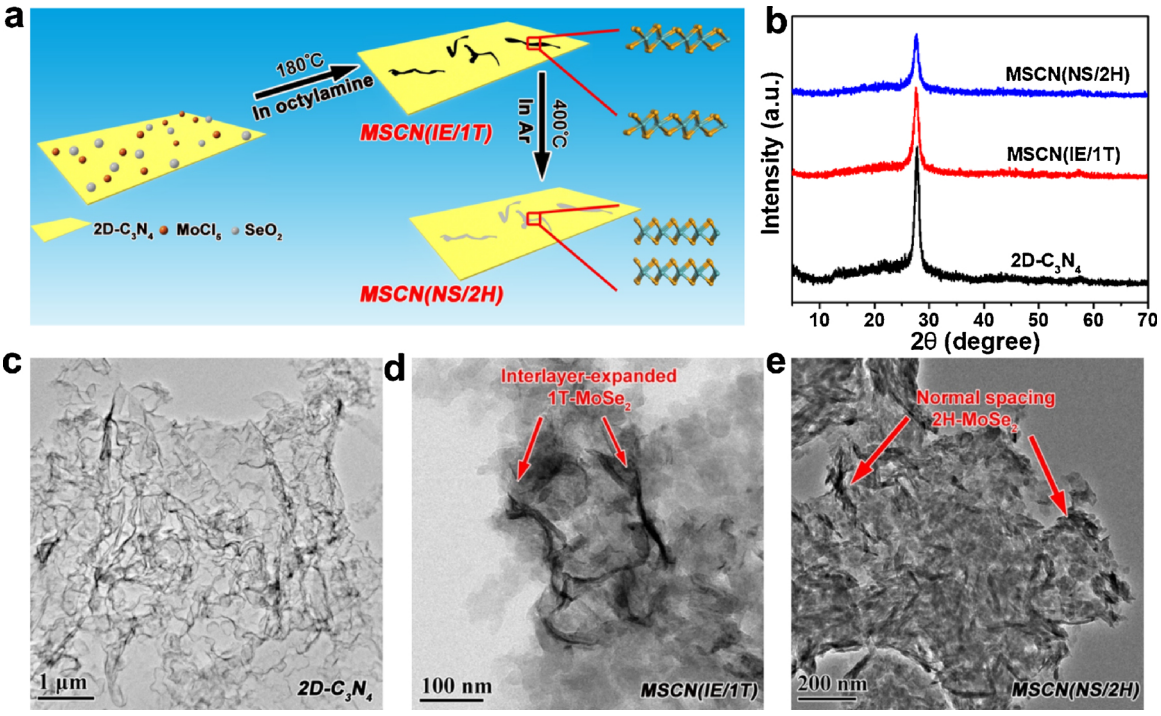

Fig. 1. (a) Schematic of the synthetic process of MSCN(IE/1T) and MSCN(NS/2H) hybrids. (b) XRD patterns of the hybrids. (c–e) TEM images of pure 2D-C_3N_4, MSCN (IE/1T) and MSCN(NS/2H) hybrids.

$MoSe_2$ cocatalyst is successfully prepared. Notably, with the annealing treatment (400°C), the interlayer-expanded $MoSe_2$ shows a reduced interlayer spacing of 0.65 nm (Fig. 2b), corresponding to the normal spacing value of pristine $MoSe_2$. The thermogravimetric (TG) analysis of pure interlayer-expanded $MoSe_2$ shows obvious weight loss from 280 to 400°C (Fig. 2c), indicating that the reduction of interlayer spacing is probably due to the loss of some intercalated molecules after annealing treatment. To find out whether octylamine affect the interlayer spacing of $MoSe_2$, the samples were then characterized using the fourier transform infrared spectrometer (FT-IR) as illustrated in Fig. 2d. It can

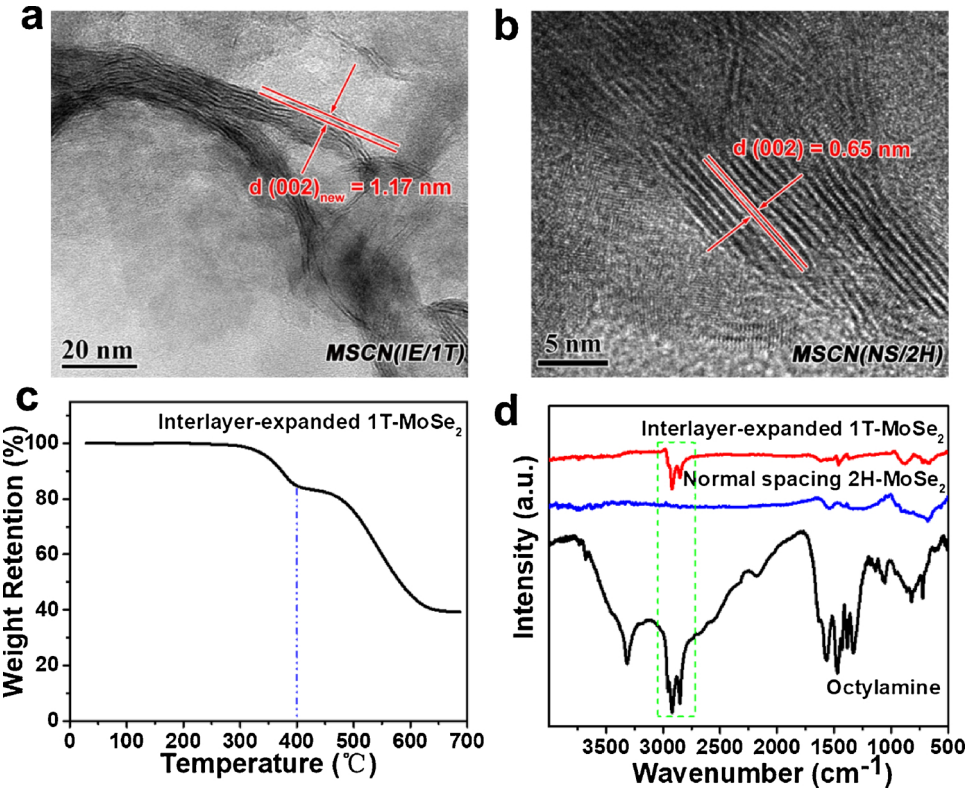

Fig. 2. (a, b) HRTEM images of MSCN(IE/1T) and MSCN(NS/2H). (c) TG curve of pure interlayer-expanded 1T-$MoSe_2$. (d) FT-IR spectrum of pure interlayer-expanded 1T-$MoSe_2$ and normal spacing 2H-$MoSe_2$ obtained by annealing the former sample.

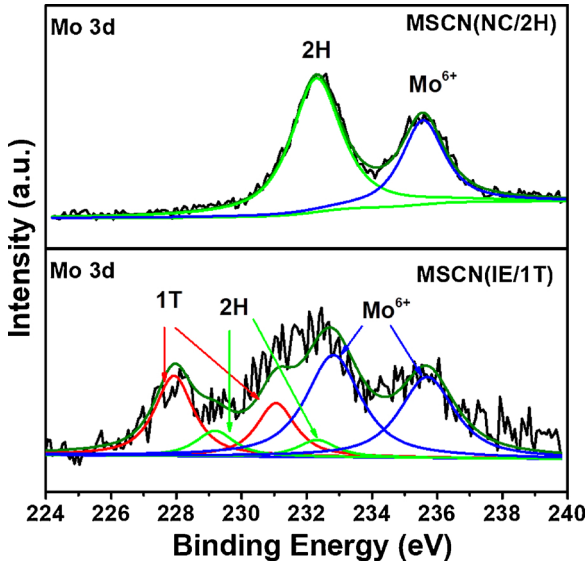

Fig. 3. Mo 3d high-resolution XPS spectra of the MSCN(IE/1T) and MSCN(NS/2H).

be found that the octylamine molecules attached on MS(IE/1T) were extracted after annealing. As such, it could be deduced that the larger interlayer distance has definite relation to the intercalation of octylamine. A periodic density functional theory (DFT) calculation was also performed to understand the increase of the $MoSe_2$ interlayer at atomic level, and the theoretical interlayer spacing of $MoSe_2$ intercalated with amine molecules is also close to the experimental result (Fig. S5).

Upon confirming the interlayer-expanded structure, the analysis of phase structure of the catalysts was then focused on. The XPS analysis is employed because it is sensitive to the surface of materials, where $MoSe_2$ cocatalysts are loaded on. Fig. 3 shows the Mo 3d high-resolution spectra of MSCN(IE/1T) and MSCN(NS/2 H). It is clear that the characteristic peaks are obviously different. The peaks of MSCN(IE/1T) show significantly shift to low energy region in contrast to MSCN(NS/2 H), which is a remarkable feature of phase transition from 2H to 1T [13,16]. According to the deconvolution of the XPS data, the peaks located at 227.8 eV and 231.0 eV for the signal of 1T phase and the peaks located at 229.4 eV and 232.3 eV for the signal of 2H phase can all be observed in the MSCN(IE/1T) sample [13,29,30], and the 1T phase content can be calculated of ca. 70%. In contrast, the spectrum of MSCN(NS/2H) only exhibits the characteristic peak ascribed to 2H phase, suggesting that the phase transition from 1T to 2H phase occurs during annealing. Theoretically, the electron donor is required to transfer electron into the d orbit of Mo atoms to form the octahedral coordination (1T phase) [15,34]. In the previous work, lithium compound [34], NH_4^+ [35], $NaBH_4$ [29] and hydrazine hydrate [36] have been demonstrated to induce phase transition to metallic 1T phase. In this work, the attached octylamine (R-NH_2) with electron rich functional group, may not just increase the interlayer spacing, or even serve as an electron donor to transfer electrons to $MoSe_2$ during the synthetic process. For this purpose, a theoretical model of $MoSe_2$ attached with amine molecules was constructed (Fig. S5). On the basis of the theoretical analysis, the Mo atoms could gain extra electrons after introducing amine molecules. The result could demonstrate that the origin of the phase transition is strongly affected by the introduction of octylamine as electron donor. Moreover, the XPS spectra of other elements in MSCN(IE/1T) are all in agreement with that of g-C_3N_4 and $MoSe_2$ [29,30,37–39] (Fig. S6).

Upon acquiring the fine structures, the photoelectrical properties were then further investigated. Indeed, the light harvesting and charge transfer are two important parameters limiting the photocatalytic reaction. As displayed in Fig. 4a, the visible light harvesting capacity of as-prepared MSCN(IE/1T) catalysts all gradually enhanced with the increased loading amount of $MoSe_2$ with black color. The MSCN(IE/1T) and MSCN(NS/2H) catalysts show similar absorption spectra as illustrated in Fig. 4b, indicating that the presented two catalysts possess comparable light harvesting capacity. To exam the charge kinetics, the time-resolved Photoluminescence (PL) spectra, and photocurrent response of the prepared hybrids were measured (Fig. 4c, d). The faster decay of the PL (shorter lifetime) means faster consumption rate of electrons and can reflect the charge separation efficiency [4,40,41]. Obviously, as illustrated in Fig. 4c, both the MSCN(IE/1T) and MSCN(NS/2H) catalysts show enhanced charge separation efficiency in comparison with bare 2D-C_3N_4, demonstrating the electron tarp role of $MoSe_2$ cocatalysts. The PL lifetime of bare 2D-C_3N_4 decrease from 4.84 ns to 3.09 and 2.98 ns for MSCN(NS/2H) and MSCN(IE/1T), respectively, indicating that the charge transfer efficiency of MSCN(IE/1T) is close to that of MSCN(NS/2H). The photocurrent responses of all the samples increase with the loading of $MoSe_2$ regardless of the phase and interlayer structure, similar to the results of time-resolved PL (Fig. 4d). Given the closed photocurrent response intensity, the comparable charge transfer efficiency of the MSCN(IE/1T) and MSCN(NS/2H) can be further evidenced. In principle, owing to the metallic feature of 1T phase, the MSCN(IE/1T) should exhibit significantly higher charge separation efficiency. The comparable charge kinetics can be ascribed to the further increased interfacial contract between 2D-C_3N_4 and MS(NC/2H) after annealing treatment [42].

Having confirmed the structure, light absorbance and charge separation efficiency of the catalysts, we are now in a position to investigate their photocatalytic hydrogen evolution activity. Obviously, under light illumination, the MSCN(IE/1T) exhibits giant enhanced photocatalytic hydrogen evolution activity compared to bare 2D-C_3N_4 (Fig. 5a), and the optimal loading amount is estimated to be 2 wt%. The lower loading amount of $MoSe_2$ will decrease the amount of active component, while a higher loading amount contributes to the light shielding effect and induce the aggregation of $MoSe_2$ on the surface. In Fig. 5b, under the same loading amount of $MoSe_2$ cocatalysts, the MSCN(IE/1T) show significantly higher HER performance (1672.6 μmol g^{-1} h^{-1}) than MSCN(NS/2H) (186.7 μmol g^{-1} h^{-1}). Given the comparable light absorbance and charge kinetics, the enhanced performance can be ascribed to the difference in the catalytic conversion step due to the different phase and interlayer structure of $MoSe_2$. On one hand, the metallic 1T phase $MoSe_2$ can provide additional active sites on the basal plane where is catalytic insert for semiconducting 2H phase $MoSe_2$ [11,19,43]. On the other hand, the interlayer-expanded structure can further optimize the H* adsorption ability on edge sites [21–23]. As such, thanks to the synergistic phase and interlayer effect benefiting the surface hydrogen adsorption/desorption process, the MSCN(IE/1T) exhibits an order of magnitude higher performance than MSCN(NS/2H). It is interesting that, even integrating the MS(IE/1T) with 2D-C_3N_4 using a simple mechanical mixing method (denoted as MSCN(IE/1T-G)) [20,33], the performance can exceed that of MSCN (NS/2H). Given the poor interface quality of MSCN(IE/1 T-G) in comparison with MSCN(NS/2H), the higher HER performance can further demonstrate the superiority of presented interlayer-expanded 1T-$MoSe_2$ cocatalyst. The performance of MSCN(IE/1T-G) is unsatisfactory compared to MSCN(IE/1T), which is mainly due to the weak bonding against the charge transfer from semiconductor to cocatalyst originated from such physical mixing assembly method. Taken together, it can be summarized that both the high-quality interfacial contact and optimized structure of cocatalyst are of great importance for the establishment of high-efficiency catalyst-semiconductor system. Regarding the stability, the MSCN(IE/1T) and MSCN(NS/2H) could last over 20 h without obvious decay, whereas the MSCN(IE/1T-G) shows a degree of decrease due to the weak bonding between photoharvester and cocatalyst (Fig. 5c).

On the basis of the observation that the wavelength-dependent hydrogen evolution yield matches well with the light absorption

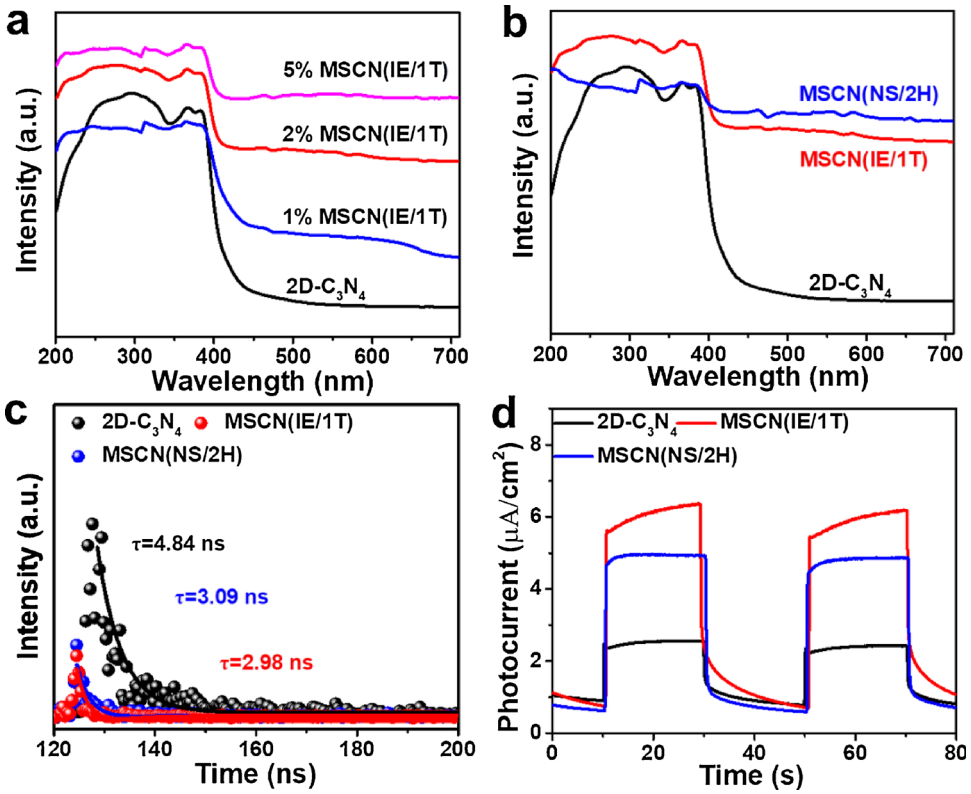

Fig. 4. (a) UV–vis absorption spectra of pure 2D-C_3N_4 and MSCN(IE/1T) hybrids with different loading amount of $MoSe_2$. (b) UV–vis absorption spectra of pure 2D-C_3N_4, MSCN(IE/1T) and MSCN(NS/2H) hybrids. (c) Time-resolved PL spectra of pure 2D-C_3N_4 and the hybrids excited at 337 nm. (d) Photocurrent vs. time (I-t) curves of the catalysts at a −0.2 V vs. Ag/AgCl under visible light irradiation.

capacity of 2D-C_3N_4, not with that of MSCN(IE/1T) (Fig. 5d), it can be deduced that the photogenerated electrons come from the 2D-C_3N_4, and $MoSe_2$ consume the electrons to catalyze the evolution of H_2. The external quantum efficiency (EQE) of as-designed MSCN(IE/1T) at 420 nm arrives at 5.2% which is the first-rank performance in g-C_3N_4 based materials using noble-metal-free cocatalysts for HER (Table S1). The superiority of the designed cocatalyts, MS(IE/1T), is further demonstrated by the higher activity than those of 2D-C_3N_4 combined with other noble-metal-free cocatalysts (i.e. MoS_2, WS_2, CNTs) or noble-metal-based materials (i.e. Au, Ag, Pd), except for Pt (Fig. S9). The result of photocatalytic hydrogen evolution strongly demonstrates the superiority of the presented phase and interlayer engineering strategy on $MoSe_2$ cocatalyst.

To further understand the interfacial charge transfer in MSCN(IE/

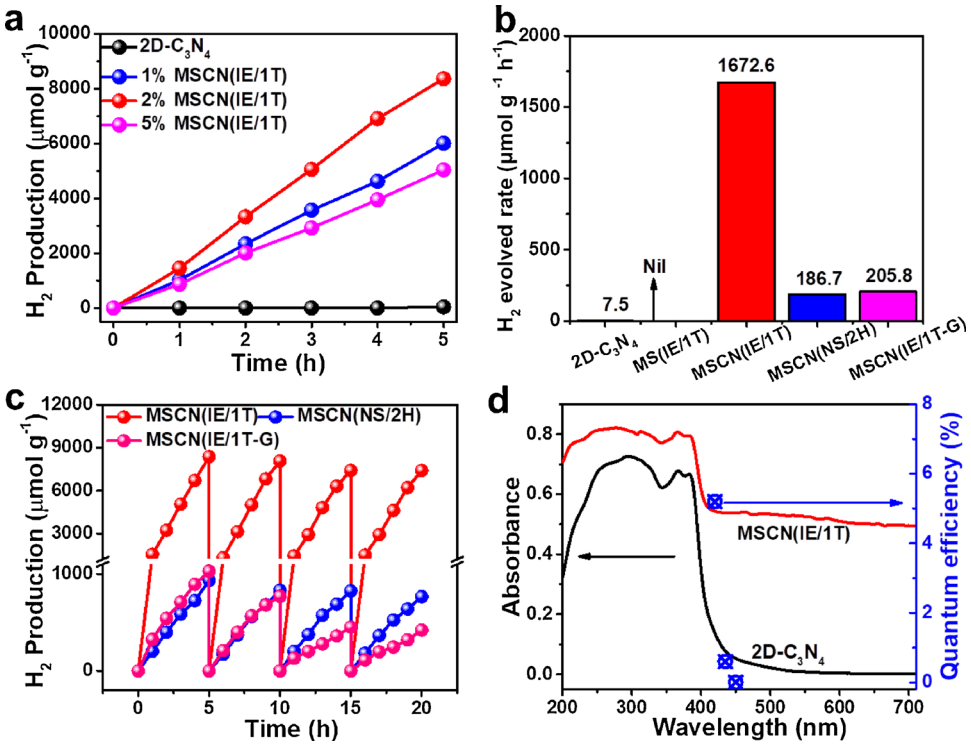

Fig. 5. (a) Photocatalytic hydrogen evolution performance of pure 2D-C_3N_4 and MSCN(IE/1T) hybrid with different loading amounts of $MoSe_2$ cocatalyst under visible light irradiation. (b) The comparison of hydrogen generation rate between pure 2D-C_3N_4, MS(IE/1T), MSCN(IE/1T), MSCN(NS/2H) and MSCN(IE/1T-G). (c) Photocatalytic stability tests of the hybrids. (d) Wavelength dependence hydrogen evolution quantum yield of MSCN(IE/1T).

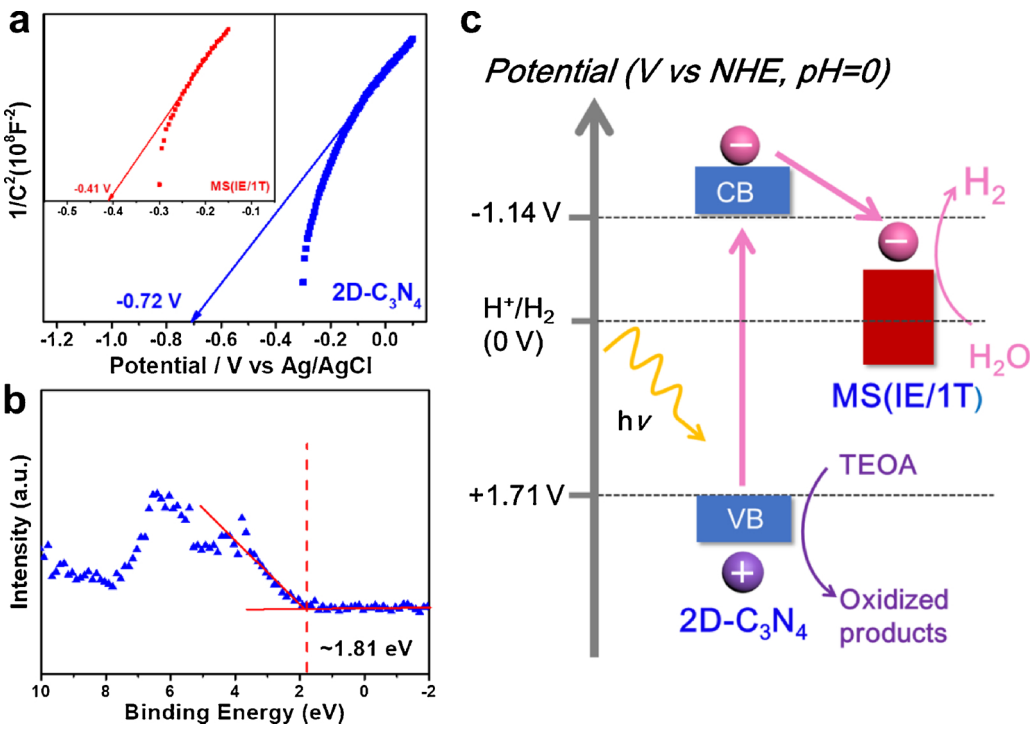

Fig. 6. (a) Mott-Schottky plots of 2D-C_3N_4 and MS(IE/1T) in 0.2 M Na_2SO_4 aqueous solution. (b) Valenceband XPS (VB-XPS) spectrum of 2D-C_3N_4. (c) Schematic of catalytic hydrogen evolution process.

1T), we combine the Valenceband XPS (VB-XPS) spectrum, Mott-Schottky pots and UV–vis absorption spectra altogether to determine the CB, VB edge position of 2D-C_3N_4 and charge migration pathway. The Mott-Schottky pots (Fig. 6a) of MS(IE/1T) display a more negative flat band position than that of 2D-C_3N_4, indicating that the electron transfer from 2D-C_3N_4 to MS(IE/1T) is thermodynamically more favourable [1]. As the $MoSe_2$ is metallic material displaying no ability to generate electron-hole pairs, it can be concluded that the 2D-C_3N_4 offers electrons and these electrons can be trapped by MS(IE/1T) to catalyze the generation of H_2, further confirming the discussion about wavelength-dependent hydrogen evolution yield. The flat band potential of 2D-C_3N_4 is measured at −0.72 V vs. Ag/AgCl, corresponding −0.1 V vs. NHE, pH = 0. In combination with the VB-XPS result (Fig. 6b), it could be calculated that the VB position of 2D-C_3N_4 locate at +1.71 V vs. NHE [6]. Given the band gap of 2.85 eV for 2D-C_3N_4 (Fig. S11), the CB position is measured to be −1.14 V vs. NHE, pH = 0. In terms of the catalytic mechanism, upon light irradiation, the photo-excited electrons in 2D-C_3N_4 will migrate to MS(IE/1T) cocatalyst though the tight interface, whilst the holes are consumed by sacrificial agent (TEOA), thereby achieving efficient charge separation. At last, owing to the excellent charge mobility and favorable hydrogen adsorption/desorption free energy of MS(IE/1T), the electrons would swiftly transfer to the abundant active sites, and reduce protons to generate hydrogen gas product (Fig. 6c).

4. Conclusions

In summary, phase and interlayer engineering were performed on the noble-metal-free $MoSe_2$ cocatalyst to boost the photocatalytic performance in hydrogen evolution. The integration of MS(IE/1T) cocatalyst with 2D-C_3N_4 leads to a dramatically enhanced HER performance of 1672.6 μmol g^{-1} h^{-1} and an external quantum efficiency of 5.2% at 420 nm. The key factor affecting such high efficiency can be ascribed to the optimized plentiful active centers of MS(IE/1T) with rational structure optimization, together with the charge extraction ability. Such synergistic phase and interlayer engineering may open a new path to improve the performance of TMDs materials, and give insight on rational design of high-efficiency photocatalytic water splitting systems. It should also be noticed that, in this work, the specific contribution from the phase or interlayer engineering is still not clear, and the as-prepared 1T-$MoSe_2$ is the mixture of 1T and 2H phase instead of pure 1T phase, both of which are significant to make further research in the future.

Acknowledgements

This study was financially supported by National Nature Science Foundation of China (21776118), China Postdoctoral Science Foundation (2017M620193), Natural Science Foundation of Jiangsu Province (BK20180870), High-tech Research Key laboratory of Zhenjiang (SS2018002), A Project Funded by the Priority Academic Program Development of Jiangsu Higher Education Institutions. This study was supported by the high performance computing platform of Jiangsu University.

Appendix A. Supplementary data

Supplementary material related to this article can be found, in the online version, at doi:https://doi.org/10.1016/j.apcatb.2018.10.054.

References

[1] J. Li, G. Zhan, Y. Yu, L. Zhang, Superior visible light hydrogen evolution of Janus bilayer junctions via atomic-level charge flow steering, Nat. Commun. 7 (2016) 11480.
[2] S. Park, W.J. Chang, C.W. Lee, S. Park, H.-Y. Ahn, K.T. Nam, Photocatalytic hydrogen generation from hydriodic acid using methylammonium lead iodide in dynamic equilibrium with aqueous solution, Nat. Energy 2 (2016) 16185.
[3] S. Bai, J. Jiang, Q. Zhang, Y. Xiong, Steering charge kinetics in photocatalysis: intersection of materials syntheses, characterization techniques and theoretical simulations, Chem. Soc. Rev. 44 (2015) 2893–2939.
[4] H. Xu, J. Yi, X. She, Q. Liu, L. Song, S. Chen, Y. Yang, Y. Song, R. Vajtai, J. Lou, H. Li, S. Yuan, J. Wu, P.M. Ajayan, 2D heterostructure comprised of metallic 1T-MoS_2 /monolayer O-g-C_3N_4 towards efficient photocatalytic hydrogen evolution, Appl. Catal. B: Environ. 220 (2018) 379–385.

[5] J. Ran, G. Gao, F.-T. Li, T.-Y. Ma, A. Du, S.-Z. Qiao, Ti_3C_2 MXene co-catalyst on metal sulfide photo-absorbers for enhanced visible-light photocatalytic hydrogen production, Nat. Commun. 8 (2017) 13907.

[6] J. Ran, B. Zhu, S.Z. Qiao, Phosphorene Co-catalyst advancing highly efficient visible-light photocatalytic hydrogen production, Angew. Chem. Int. Ed. 56 (2017) 10373–10377.

[7] W. Jiang, S. Bai, L. Wang, X. Wang, L. Yang, Y. Li, D. Liu, X. Wang, Z. Li, J. Jiang, Y. Xiong, Integration of multiple plasmonic and co-catalyst nanostructures on TiO_2 nanosheets for visible-near-infrared photocatalytic hydrogen evolution, Small 12 (2016) 1640–1648.

[8] S. Huang, Y. Xu, M. Xie, Y. Ma, J. Yan, Y. Li, Y. Zhao, H. Xu, H. Li, Multifunctional C-Doped $CoFe_2O_4$ material as cocatalyst to promote reactive oxygen species generation over magnetic recyclable C–CoFe/Ag–AgX photocatalysts, ACS Sustain. Chem. Eng. 6 (2018) 11968–11978.

[9] S. Bai, Y. Xiong, Some recent developments in surface and interface design for photocatalytic and electrocatalytic hybrid structures, Chem. Commun. 51 (2015) 10261–10271.

[10] J. Ran, J. Zhang, J. Yu, M. Jaroniec, S.Z. Qiao, Earth-abundant cocatalysts for semiconductor-based photocatalytic water splitting, Chem. Soc. Rev. 43 (2014) 7787–7812.

[11] K. Chang, X. Hai, J. Ye, Transition metal disulfides as noble-metal-alternative Co-catalysts for solar hydrogen production, Adv. Energy Mater. 6 (2016) 1502555.

[12] B. Hinnemann, P.G. Moses, J. Bonde, K.P. Jørgensen, J.H. Nielsen, S. Horch, I. Chorkendorff, J.K. Nørskov, Biomimetic hydrogen evolution: MoS_2 nanoparticles as catalyst for hydrogen evolution, J. Am. Chem. Soc. 127 (2005) 5308–5309.

[13] Y. Yu, G.H. Nam, Q. He, X.J. Wu, K. Zhang, Z. Yang, J. Chen, Q. Ma, M. Zhao, Z. Liu, F.R. Ran, X. Wang, H. Li, X. Huang, B. Li, Q. Xiong, Q. Zhang, Z. Liu, L. Gu, Y. Du, W. Huang, H. Zhang, High phase-purity 1T'-MoS_2- and 1T'-$MoSe_2$-layered crystals, Nat. Chem. 10 (2018) 638–643.

[14] G. Ye, Y. Gong, J. Lin, B. Li, Y. He, S.T. Pantelides, W. Zhou, R. Vajtai, P.M. Ajayan, Defects engineered monolayer MoS_2 for improved hydrogen evolution reaction, Nano Lett. 16 (2016) 1097–1103.

[15] M. Chhowalla, H.S. Shin, G. Eda, L.-J. Li, K.P. Loh, H. Zhang, The chemistry of two-dimensional layered transition metal dichalcogenide nanosheets, Nat. Chem. 5 (2013) 263–275.

[16] D. Voiry, H. Yamaguchi, J. Li, R. Silva, D.C. Alves, T. Fujita, M. Chen, T. Asefa, V.B. Shenoy, G. Eda, M. Chhowalla, Enhanced catalytic activity in strained chemically exfoliated WS_2 nanosheets for hydrogen evolution, Nat. Mater. 12 (2013) 850–855.

[17] D. Voiry, A. Mohite, M. Chhowalla, Phase engineering of transition metal dichalcogenides, Chem. Soc. Rev. 44 (2015) 2702–2712.

[18] K. Chang, X. Hai, H. Pang, H. Zhang, L. Shi, G. Liu, H. Liu, G. Zhao, M. Li, J. Ye, Targeted synthesis of 2H- and 1T-Phase MoS_2 monolayers for catalytic hydrogen evolution, Adv. Mater. 28 (2016) 10033–10041.

[19] D. Voiry, J. Yang, M. Chhowalla, Recent strategies for improving the catalytic activity of 2D TMD nanosheets toward the hydrogen evolution reaction, Adv. Mater. 28 (2016) 6197–6206.

[20] J. Yi, X. She, Y. Song, M. Mao, K. Xia, Y. Xu, Z. Mo, J. Wu, H. Xu, H. Li, Solvothermal synthesis of metallic 1T-WS_2: a supporting co-catalyst on carbon nitride nanosheets toward photocatalytic hydrogen evolution, Chem. Eng. J. 335 (2018) 282–289.

[21] J. Xu, J. Zhang, W. Zhang, C.-S. Lee, Interlayer nanoarchitectonics of two-dimensional transition-metal dichalcogenides nanosheets for energy storage and conversion applications, Adv. Energy Mater. 7 (2017) 1700571.

[22] M.R. Gao, M.K. Chan, Y. Sun, Edge-terminated molybdenum disulfide with a 9.4-a interlayer spacing for electrochemical hydrogen production, Nat. Commun. 6 (2015) 7493.

[23] Y.-J. Tang, Y. Wang, X.-L. Wang, S.-L. Li, W. Huang, L.-Z. Dong, C.-H. Liu, Y.-F. Li, Y.-Q. Lan, Molybdenum disulfide/nitrogen-doped reduced graphene oxide nanocomposite with enlarged interlayer spacing for electrocatalytic hydrogen evolution, Adv. Energy Mater. 6 (2016) 1600116.

[24] K. Chang, Z. Mei, T. Wang, Q. Kang, S. Ouyang, J. Ye, MoS_2/graphene cocatalyst for efficient photocatalytic H_2 evolution under visible light irradiation, ACS Nano 8 (2014) 7078–7087.

[25] S. Bai, L. Wang, X. Chen, J. Du, Y. Xiong, Chemically exfoliated metallic MoS_2nanosheets: a promising supporting co-catalyst for enhancing the photocatalytic performance of TiO_2 nanocrystals, Nano Res. 8 (2014) 175–183.

[26] Q. Liu, Q. Shang, A. Khalil, Q. Fang, S. Chen, Q. He, T. Xiang, D. Liu, Q. Zhang, Y. Luo, L. Song, In situ integration of a metallic 1T-MoS_2/CdS heterostructure as a means to promote visible-light-driven photocatalytic hydrogen evolution, ChemCatChem 8 (2016) 2614–2619.

[27] S. Xu, Z. Lei, P. Wu, Facile preparation of 3D MoS_2/$MoSe_2$ nanosheet–graphene networks as efficient electrocatalysts for the hydrogen evolution reaction, J. Mater. Chem. A 3 (2015) 16337–16347.

[28] Y. Qu, H. Medina, S.-W. Wang, Y.-C. Wang, C.-W. Chen, T.-Y. Su, A. Manikandan, K. Wang, Y.-C. Shih, J.-W. Chang, H.-C. Kuo, C.-Y. Lee, S.-Y. Lu, G. Shen, Z.M. Wang, Y.-L. Chueh, Wafer scale phase-engineered 1T- and 2H-$MoSe_2$/Mo core-shell 3D-hierarchical nanostructures toward efficient electrocatalytic hydrogen evolution reaction, Adv. Mater. 28 (2016) 9831–9838.

[29] Y. Yin, Y. Zhang, T. Gao, T. Yao, X. Zhang, J. Han, X. Wang, Z. Zhang, P. Xu, P. Zhang, X. Cao, B. Song, S. Jin, Synergistic phase and disorder engineering in 1T-$MoSe_2$ nanosheets for enhanced hydrogen-evolution reaction, Adv. Mater. 29 (2017) 1700311.

[30] M. Jiang, J. Zhang, M. Wu, W. Jian, H. Xue, T.-W. Ng, C.-S. Lee, J. Xu, Synthesis of 1T-$MoSe_2$ ultrathin nanosheets with an expanded interlayer spacing of 1.17 nm for efficient hydrogen evolution reaction, J. Mater. Chem. A 4 (2016) 14949–14953.

[31] Z.-T. Shi, W. Kang, J. Xu, Y.-W. Sun, M. Jiang, T.-W. Ng, H.-T. Xue, D.Y.W. Yu, W. Zhang, C.-S. Lee, Hierarchical nanotubes assembled from MoS_2 -carbon monolayer sandwiched superstructure nanosheets for high-performance sodium ion batteries, Nano Energy 22 (2016) 27–37.

[32] Q. Liu, X. Li, Q. He, A. Khalil, D. Liu, T. Xiang, X. Wu, L. Song, Gram-scale aqueous synthesis of stable few-layered 1T-MoS_2: applications for visible-light-driven photocatalytic hydrogen evolution, Small 11 (2015) 5556–5564.

[33] B. Mahler, V. Hoepfner, K. Liao, G.A. Ozin, Colloidal synthesis of 1T-WS_2 and 2H-WS_2 nanosheets: applications for photocatalytic hydrogen evolution, J. Am. Chem. Soc. 136 (2014) 14121–14127.

[34] D. Voiry, M. Salehi, R. Silva, T. Fujita, M. Chen, T. Asefa, V.B. Shenoy, G. Eda, M. Chhowalla, Conducting MoS_2 nanosheets as catalysts for hydrogen evolution reaction, Nano Lett. 13 (2013) 6222–6227.

[35] Q. Liu, X. Li, Z. Xiao, Y. Zhou, H. Chen, A. Khalil, T. Xiang, J. Xu, W. Chu, X. Wu, J. Yang, C. Wang, Y. Xiong, C. Jin, P.M. Ajayan, L. Song, Stable metallic 1T-WS_2 nanoribbons intercalated with Ammonia ions: the correlation between structure and electrical/optical properties, Adv. Mater. 27 (2015) 4837–4844.

[36] H. Li, S. Chen, X. Jia, B. Xu, H. Lin, H. Yang, L. Song, X. Wang, Amorphous nickel-cobalt complexes hybridized with 1T-phase molybdenum disulfide via hydrazine-induced phase transformation for water splitting, Nat. Commun. 8 (2017) 15377.

[37] X. She, J. Wu, J. Zhong, H. Xu, Y. Yang, R. Vajtai, J. Lou, Y. Liu, D. Du, H. Li, P.M. Ajayan, Oxygenated monolayer carbon nitride for excellent photocatalytic hydrogen evolution and external quantum efficiency, Nano Energy 27 (2016) 138–146.

[38] Z. Mo, H. Xu, Z. Chen, X. She, Y. Song, J. Wu, P. Yan, L. Xu, Y. Lei, S. Yuan, H. Li, Self-assembled synthesis of defect-engineered graphitic carbon nitride nanotubes for efficient conversion of solar energy, Appl. Catal. B: Environ. 225 (2018) 154–161.

[39] X. She, J. Wu, H. Xu, Z. Mo, J. Lian, Y. Song, L. Liu, D. Du, H. Li, Enhancing charge density and steering charge unidirectional flow in 2D non-metallic semiconductor-CNTs-metal coupled photocatalyst for solar energy conversion, Appl. Catal. B: Environ. 202 (2017) 112–117.

[40] J.-X. Li, C. Ye, X.-B. Li, Z.-J. Li, X.-W. Gao, B. Chen, C.-H. Tung, L.-Z. Wu, A redox shuttle accelerates O_2 evolution of photocatalysts formed in situ under visible light, Adv. Mater. 29 (2017) 1606009.

[41] G. Zhao, Y. Sun, W. Zhou, X. Wang, K. Chang, G. Liu, H. Liu, T. Kako, J. Ye, Superior photocatalytic H_2 production with cocatalytic Co/Ni species anchored on sulfide semiconductor, Adv. Mater. 29 (2017) 1703258.

[42] Y. Zhu, Z. Xu, Q. Lang, W. Jiang, Q. Yin, S. Zhong, S. Bai, Grain boundary engineered metal nanowire cocatalysts for enhanced photocatalytic reduction of carbon dioxide, Appl. Catal. B: Environ. 206 (2017) 282–292.

[43] H. Li, X. Jia, Q. Zhang, X. Wang, Metallic transition-metal dichalcogenide nanocatalysts for energy conversion, Chem 4 (2018) 1510–1537.